Tribology Letters (2021) 69:19
https://doi.org/10.1007/s11249-020-01385-8

ORIGINAL PAPER

Tribological Performance of Magnesium Silicate Hydroxide/Ni Composite as an Oil-Based Additive for Steel–Steel Contact

Yuan Qin[1] · Mingxia Wu[1] · Gang Yang[1] · Yi Yang[1] · Leiming Zhao[1]

Received: 12 August 2020 / Accepted: 28 November 2020 / Published online: 20 January 2021

Abstract

Synthetic MSH can solve the shortcomings of natural, self-repairing serpentine materials, but its tribological properties are not ideal. Herein, Ni was selected as an accelerant to prepare MSH/Ni composite powder to obtain better friction performance. The tribological performance of MSH/Ni was investigated using ball-disk wear tests, and the worn surfaces were characterized by SEM, EDS, WLI, and XPS. The results suggest that the tribological properties of the MSH/Ni composite are better than those of MSH and Ni, and the base oil wear scar area can be reduced by 78.13%. The excellent friction performance of MSH/Ni composite powder was attributed to the rolling bearing effect of Ni under low load, and the self-repairing effect of MSH under high load. Surface analysis demonstrated that as a lubricant additive, MSH/Ni can form a smoother tribofilm mainly composed of Fe_3O_4, FeOOH, SiO_x, and NiO. MSH forms a film mainly through a tribochemical reaction, while Ni particles form a film through physical means of plastic flow. Additionally, compared with commercial lubricant additives, MSH/Ni composite powder not only has better anti-wear properties but also does not corrode metal parts.

Keywords Magnesium silicate hydroxide · MSH/Ni composite · Lubricant additives · Tribological performance · Synergistic effect

1 Introduction

Lubricant additives can improve the friction performance of the base oil by changing the physical and chemical properties of the lubricating oil or the contact state between the friction pairs [1, 2]. With the advancement of modern industry, mechanical parts face more severe working conditions and require better lubrication systems. Additionally, due to environmental protection pressures, environmentally friendly lubricant additives with excellent performance must be found to replace dialkyl dithiophosphate [3], sulfide alkylphenols [4], and other traditional additives. Natural serpentine, which is a phyllosilicate mineral composed of $Mg_6(Si_4O_{10})(OH)_8$, has attracted increasing attention due to its low cost, specially layered molecular structure, and nanotubes morphology [5]. Many studies have shown that serpentine can improve the wear resistance of parts by forming a self-repairing layer containing iron oxide and silicon oxide on the worn surface [6–10]. However, natural serpentine contains impurities, such as MgO and CaO, and the impurity content of serpentine from different regions is different [11], which will affect the friction performance. Natural serpentine is highly biotoxic to human lungs, and its application is restricted in many areas [12, 13].

To solve these problems [14–16], pure and nontoxic magnesium silicate hydroxide ($Mg_6(Si_4O_{10})(OH)_8$, MSH) was synthesized, and its friction properties as lubricant additives have been studied [17, 18]. Wang et al. [19] synthesized different types of MSH by controlling the reaction time and temperature and found that the wear resistance of tubular MSH was better than that of lamellate MSH. Gao et al. [20] synthesized oleic-acid-modified MSH and found that it has better tribological properties, mainly because it can form a self-repairing layer on the friction surface. However, the friction enhancing effect of synthetic MSH is not ideal, and it is difficult to form a self-repairing layer with a micrometer thickness. Furthermore, compared with nanoparticles, the friction reduction performance of MSH is poor [19].

In recent years, many reports have confirmed the excellent friction properties of various composite additives such as graphene oxide/Fe_3O_4 [21], MoDTC/TiO_2

✉ Gang Yang
yanggang@scu.edu.cn

[1] School of Mechanical Engineering, Sichuan University, Chengdu 610065, People's Republic of China

[22], and MWCNT/Ni [23]. The tribological properties of phyllosilicate mineral composite additives have also been extensively studied [24–34], as shown in Table 1. Phyllosilicate composite additives often have better friction properties than single additives due to the synergistic effect between the phyllosilicate and the accelerant. Therefore, the preparation of the MSH composite additive is considered to be an effective means to improve the friction performance of MSH. Although there are many reports about layered silicate composite additives, the synergistic mechanism between layered silicate and other particles remains to be further studied.

In this study, to improve the friction performance of MSH, Ni particles were selected as the accelerant due to their good friction performance [35, 36] and catalytic effect [37], and the MSH/Ni composite powder was prepared by mechanical ball milling. The tribological properties of MSH nanotube/Ni composites were studied by rotating ball-disk wear tests. In addition, the worn surfaces were characterized by SEM, EDS, WLI, and XPS. Finally, combining the tribological properties of MSH/Ni composite powders under different loads, the synergistic mechanism of MSH nanotubes and Ni particles was discussed.

2 Experiment

2.1 Sample Preparation

Commercial MgO (99% purity) and $Na_2SiO_3{\cdot}9H_2O$ (99% purity) were obtained from Cologne, China. They were mixed in 800 ml aqueous NaOH (pH 13) at a certain proportion (molar ratio 3:2). Then, the suspension was placed in a 1000-ml stainless steel autoclave to react at 280 °C for 24 h. After the reaction, the suspension was cooled to room temperature naturally and repeatedly washed with distilled water to a pH of 7–8. Finally, the product was dried under vacuum at 100 °C to obtain the pure magnesium silicate hydroxide powder. Spherical Ni (> 99.9 wt%) was purchased from the China Metallurgical Research Institute. Then, the MSH nanotubes and Ni powders were mixed (mass ratios 8:2) in a high-energy planetary ball mill with a ZrO ball-to-powder weight ratio of 4:1. The composite powder was obtained by running the ball mill at 300 rpm for 8 h. The morphology of the powder was analyzed by scanning electron microscope (SEM), and the phase of the powder was analyzed by X-ray diffraction (XRD).

For stable dispersal in lubricating oil, the powder must be modified organically. The powders (MSH, Ni, and composite) were added to an alcohol solution with 10 wt% oleic

Table 1 Reported literature on phyllosilicate mineral composites as additive

Author	Year	Particles	Preparations	Findings
Du et al. [24]	2016	Muscovite/CeO_2	Mechanical solid-state chemistry reaction	Compared to Mu, μ↓5.75%, WSD↓; Ce had a catalytic effect
Wang et al. [25]	2015	Muscovite/La_2O_3	Ball-milling solid-state chemical reaction	Compared to base oil, μ↓47.6%, WSD↓11.2%
Du et al. [26]	2017	Muscovite/Cu	Liquid phase reduction	Compared to NPs, μ↓24.29%, Wv↓28.1% (estimated)
Zhao et al. [27]	2012	Serpentine/$La(OH)_3$	Sol–gel method	Compared to NPs,μ↓3.58%,WSD↓31.15%; La had a catalytic effect
Zhang et al. [28]	2013	Serpentine/La_2O_3	/	Compared to NPs, μ↓, WSD↓
Zhang et al. [29]	2011	Serpentine/Cu	Ball mill	The composite powder containing 7.5wt% Cu had the best friction performance compared to NPs, μ↓, WSD↓17.7%
Cheng et al. [30]	2018	Montmorillonite/MoS_2	Liquid precipitation	Compared to NPs, μ↓48.86%, Wv↓76.2%
Feng et al. [31]	2018	Attapulgite/La_2O_3	Ball mill	The composite powder containing 40wt% La_2O_3 had the best friction performance compared to NPs, μ↓13.85%, WR↓50.4%
Feng et al. [32]	2014	Attapulgite/Ni	Ball mill	When the mass ratio of AP and Ni was 5:1, the composite had the best friction performance. compared to NPs,μ↓14.3%,WR↓34.9%(estimated)
Wu et al. [33]	2018	Palygorskite/Cu	Liquid phase reduction	Compared to palygorskite, P_B↑9.1%
Mobasher, A et al. [34]	2020	MWCNTs/Talc	/	Compared to basic grease, μ↓63.44, WR↓80.62%

μ friction coefficient, *WSD* wear scar diameter, *WR* wear rate, *Wv* wear volume, P_B the maximal nonseizure load, *NPs* single-layered silicate additive, *estimate* estimate after measuring the data in the article figure

acid and ultrasonicated for 30 min. The resulting mixture was then dried to obtain the modified powder. Then, 0.5 wt% of the modified powder was added to the base oil and dispersed by ultrasonic dispersion for 30 min.

2.2 Tribological Tests

The tribological properties of these different additives were evaluated using the MMW-1 ball-disk friction test. The friction couple consists of three upper rotation balls (AISI 52100 steel, diameter 12.7 mm, hardness 59–61 HRC, and Ra < 0.01 μm) and a fixed disk (GB 45# steel, hardness 32–35 HRC, and Ra = 0.25–0.35 μm). Polyalphaolefin (PAO10, the viscosity was 10.1 cSt at 100 °C) was selected as the base oil, and the friction couple was completely immersed in 80 ml of the lubricating oil. Before the test, the friction couple was cleaned by ultrasonication for 10 min to eliminate the surface oil. The tribological test was carried out at room temperature for 10 h. The load was 100 N (corresponding to a maximum pressure of 1.8 GPa), and the rotation speed was 500 rpm (corresponding to a linear speed of 1.204 m/s). To ensure the accuracy and reliability of the results, each sample was repeated at least three times, and the average value was obtained. After the friction test, the friction coefficient was recorded by the computer, and the wear scars were observed by optical microscope. Then, the morphology and elemental distribution of the worn surface were analyzed using a Phenom Pro scanning electron microscope, a Bruker white light interferometer, and an ESCALAB 250Xi X-ray photoelectron spectrometer.

3 Results and Discussion

3.1 Material Characterization

The SEM images of the synthesized MSH powder, the Ni powder, and the composite powder acquired by ball milling are presented in Fig. 1. The synthesized MSH is visibly tubular with a tube length of 1–3 μm, an outer tube diameter of 20–50 nm, and an inner tube diameter of approximately 10 nm (Fig. 1a). All the Ni powders are nearly spherical with a particle size of 0.1–1.5 μm (Fig. 1b). As shown in Fig. 1c, the MSH particles are fine and agglomerate in composite powders after ball milling, while the Ni particles are almost unaffected and relatively dispersed. As seen

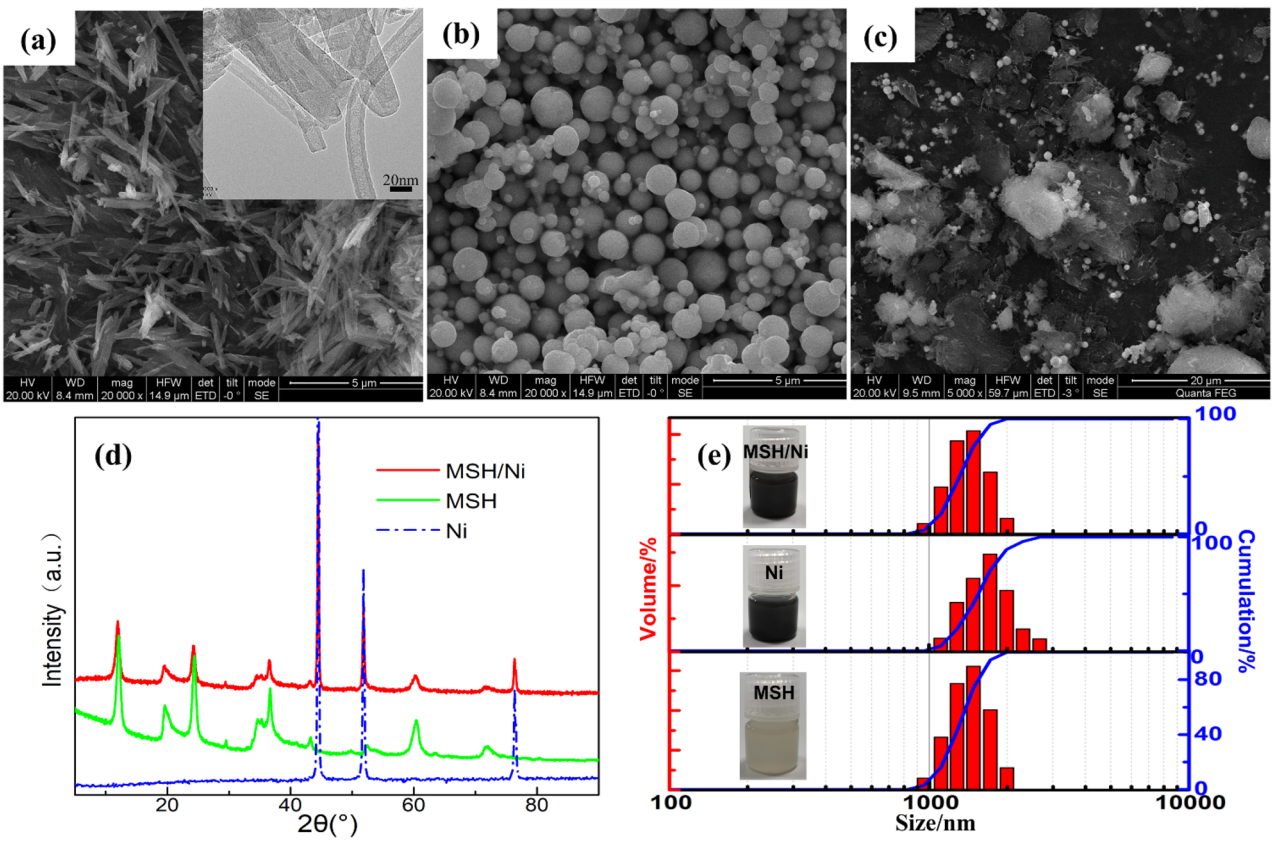

Fig. 1 Morphologies of the **a** MSH powders, **b** Ni powders, and **c** MSH/Ni powders; **d** XRD pattern and **e** particle size distribution of different powders

in Fig. 1d, the XRD patterns of the powders confirm that the synthesized MSH has a standard monoclinic structure (JCPDS Card No.10-0381). The XRD peaks of Ni at 44.51°, 51.85°, and 76.35° correspond to the (111), (200), and (220) crystal planes, respectively. No new phases were formed in the composite powder after ball milling. The particle size distribution of the different powders in the base oil is shown in Fig. 1e. The average particle sizes of the MSH, Ni, and MSH/Ni powders are 1.437 μm, 1.702 μm, and 1.423 μm, respectively. After standing for 10 h, the oil sample is well dispersed without precipitation, which ensures the dispersion of additives in the friction test.

3.2 Friction and Wear Performance

Figure 2a shows the friction coefficient curves for different oil samples. The FCs of the base oil fluctuate up and down in the first 200 min and then decrease dramatically. This is because, after the initial 200 min of severe wear, the increase in the actual contact area will lead to a decrease in the contact pressure, resulting in a decrease in the FC. In contrast, the FC of the composite additive decreased rapidly in the initial 30 min, then stabilized, and fluctuated considerably after 200 min. Compared with MSH, the friction coefficient–time curve for Ni is smoother and lower, which may be attributed to the different friction mechanisms of the two particles, as will be explored later. The average friction coefficient and average wear scar area of different additives are shown in Fig. 2b. The composite additive has the lowest average friction coefficient at 0.090 ± 0.004 and has the largest decrease (15.1%) compared to the base oil. This result shows that the MSH/Ni composite additive has a better friction reduction effect than the single additive. The average wear scar area on the rotating balls for the oil samples with MSH, MSH/Ni, and Ni are 0.40, 0.28, and 0.44 mm^2, respectively. Compared with the base oil (1.28 mm^2), the WSA value is reduced by 68.75%, 78.13%, and 65.63%, respectively. That is, the presence of lubricant additives significantly reduces the wear of the rotating ball. Notably, the composite powder exhibits excellent friction properties, which is attributed to the synergistic effect between the MSH nanotubes and the spherical Ni.

3.3 Worn Surface Analysis

The worn surface of the rotation ball was characterized by SEM and EDS, as shown in Fig. 3. For the base oil, the worn surface exhibits deep furrows, which may be caused by wear debris on the friction pair. The worn surfaces with MSH and MSH/Ni additives look smoother, especially the surface with MSH/Ni, which only has shallow furrows. The worn surface with Ni has a low-stress abrasion state, which implies that spherical Ni can be used as microbearings to convert sliding friction into rolling friction. The EDS of the base oil shows that there are Fe, Cr, O, and trace amounts of C. For the MSH sample, the contents of characteristic elements Mg and Si are 1.91 at% and 1.63 at%, respectively, which confirms that a tribofilm was formed on the worn surface. For the rubbing surface lubricated by MSH/Ni, the contents of characteristic elements Mg, Si, and Ni are 1.00 at%, 1.24 at%, and 1.71 at%, respectively. However, only a small amount of Ni (0.39 at%) can be detected on the worn surface when only Ni is added to the base oil, which indicates that Ni additive can only play the role of microbearings on the surface of the steel ball and cannot form a film.

To fully understand the "ball on disk" friction test process, the worn surface of the fixed disk was also analyzed by SEM, EDS, and optical profilometer techniques. Figure 4 shows that the worn surface lubricated with the additive is much smoother than the surface with base oil. There are

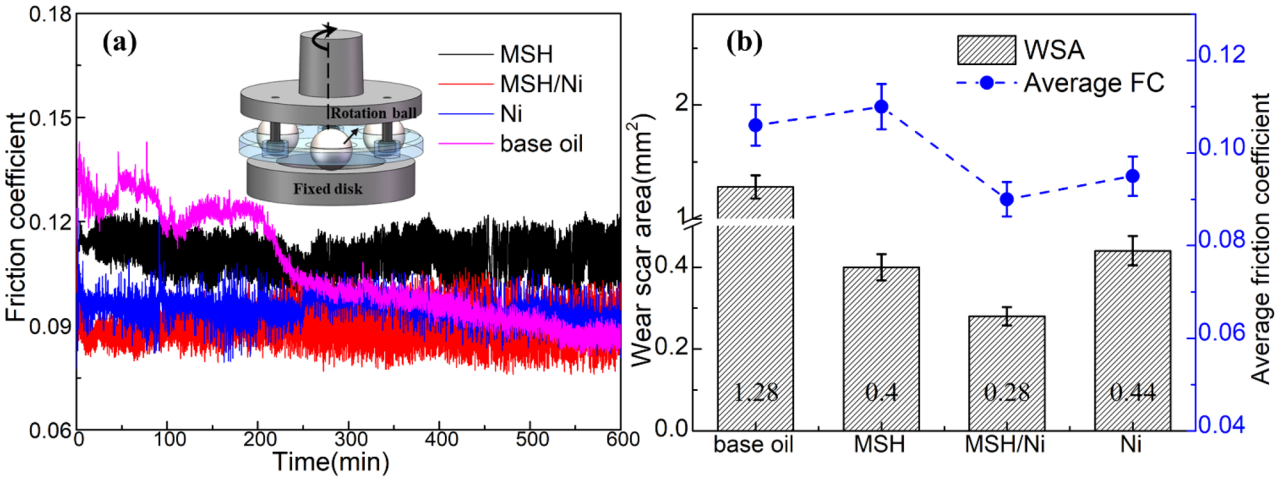

Fig. 2 **a** FC curves for different oil samples; **b** Average FC and WSA for different oil samples

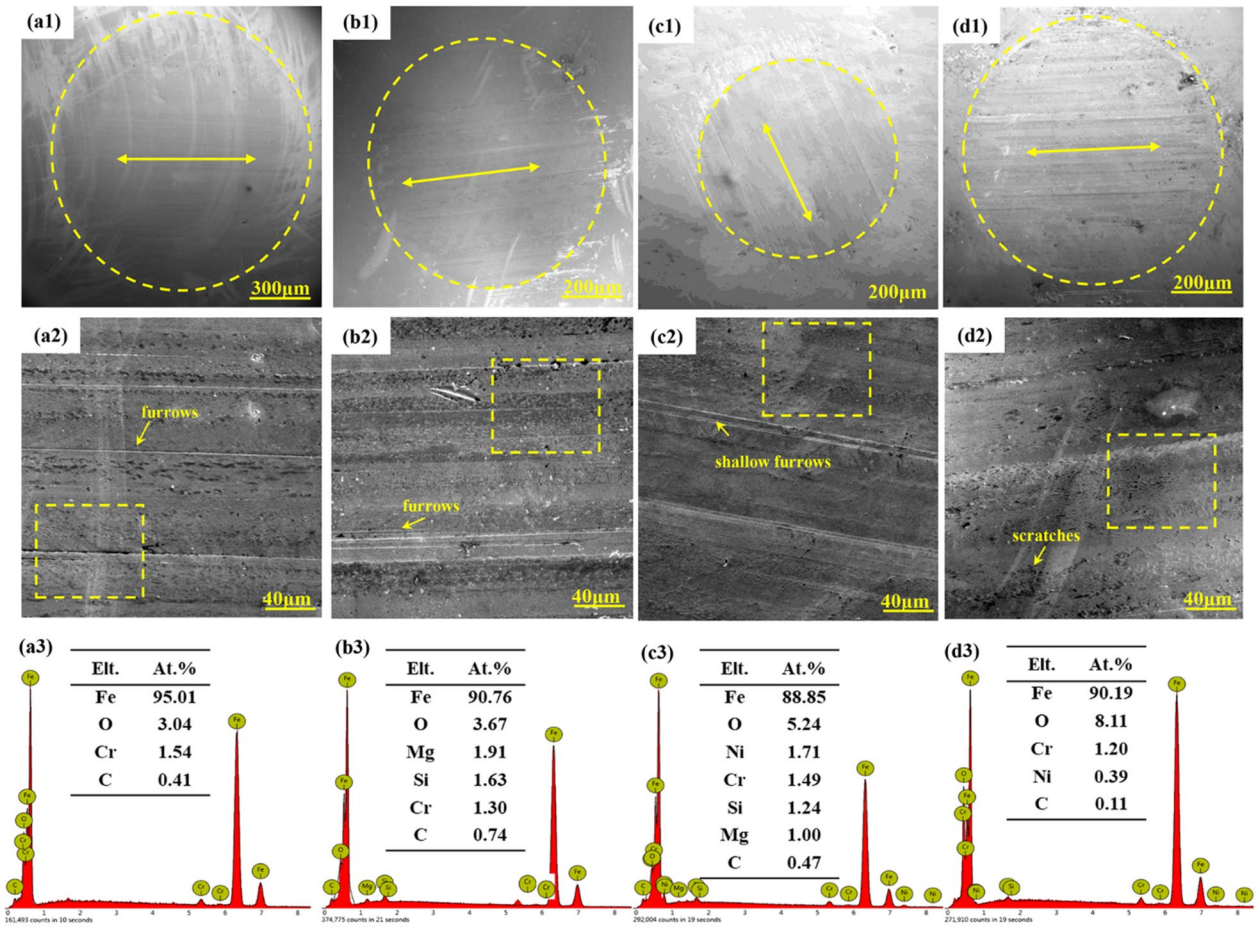

Fig. 3 SEM micrograph and EDS pattern of the worn surface of the rotation ball: **a** base oil; **b** MSH; **c** MSH/Ni; and **d** Ni

many furrows, grooves, and some burrs on the surface with base oil due to severe wear in the absence of a tribofilm. The worn surface morphology of MSH shows fewer furrows and burrs, and there are numerous micropores (a typical self-repairing morphology [9]) in the flat area, indicating the formation of the tribofilm on the surface. For the MSH/Ni composite, the rubbing surface is still very smooth with few shallow furrows. There are many pits on the worn surface lubricated by Ni, which may be related to the incomplete formation of a tribofilm. Figure 4a3–d3 shows the three-dimensional morphologies of the rubbing surfaces with different lubricating oil additives. The worn surface with the base oil has bumps and pits, and the worn surface is notably smoother after adding additives. The surface roughness with base oil, MSH, MSH/Ni, and Ni are 1.40 ± 0.16, 0.66 ± 0.04, 0.45 ± 0.02, and 0.54 ± 0.05 μm, respectively. The tribofilm formed by the MSH/Ni composite powder is the smoothest among all oil samples. The 3D images also provide a visual representation of the wear volumes of the different disks. Furthermore, according to the wear volume in this region, the disk wear volumes with the base oil, MSH, MSH/Ni, and Ni are estimated to be 0.83, 0.26, 0.22, and 0.28 mm^3, respectively. The wear rate of the disk is observed to be significantly reduced after adding additives to the base oil.

As seen from the EDS patterns (Fig. 4a2–d2), the worn surface of the disk with the base oil lubrication contains Fe, O, and C. Among them, O comes from air and C comes from the cracking deposit of the base oil [38]. In addition, after adding MSH, elemental Mg, Si, and O are detected on the surface, and elemental O is significantly increased in contrast with the base oil, which demonstrates that the worn surface of the disk formed a tribofilm with the participation of MSH. For the MSH/Ni, compared with MSH, the Mg and Si elemental content decreases, and Ni is present. This result indicates that Mg, Si, and Ni will participate in the formation of the film, and there may be a competitive relationship between Ni and MSH in the composite powder. When only Ni was added as a lubricant, 29.49 at% O and 7.26 at% Ni are detected on the worn surface, indicating that a tribofilm containing Ni and O is formed on the surface.

To further analyze the friction mechanism of the composite powder, the chemical bonding state of the worn surface of

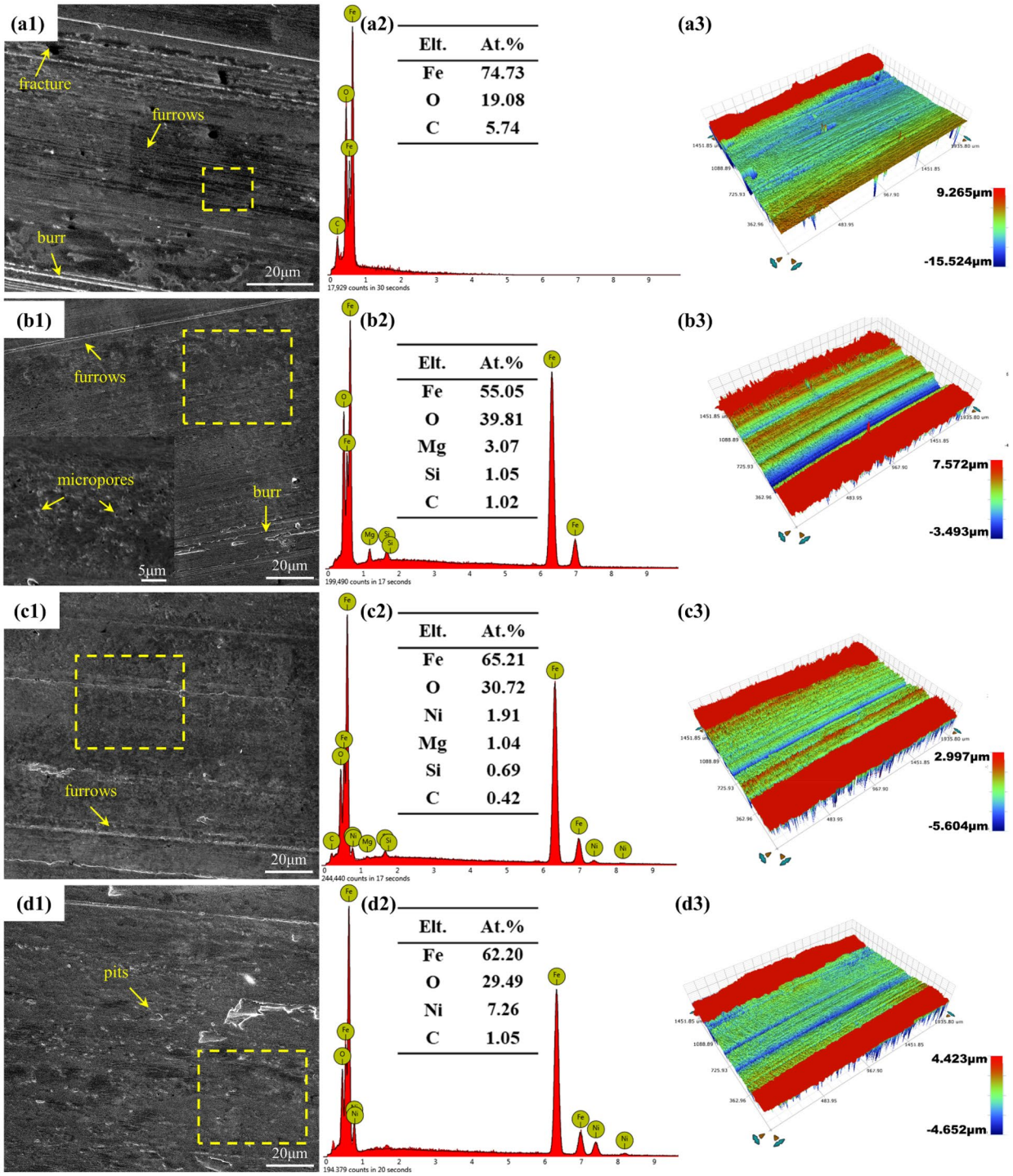

Fig. 4 SEM micrograph, EDS pattern, and 3D morphologies of the worn surface of the fixed disk: **a** base oil; **b** MSH; **c** MSH/Ni; and **d** Ni

the disk was detected by XPS. From the XPS full spectrum of the worn surface (Fig. 5a), large amounts of C and O, as well as small amounts of Fe and Si, are detected on the worn surface, indicating that there is a carbon film containing iron oxide and silicon oxide on the surface. Moreover, the C 1s spectra (Fig. 5c) are deconvoluted into three subpeaks at 284.87, 286.46, and 288.33 eV, which are assigned to C=C, C–O, and C=O, respectively. The results suggest that the carbon film on the worn surface comes from cracking and deposition of the base oil. To explore the tribofilm containing Mg and Ni, we etched the surface for 40 s and stripped approximately 20 nm from the surface. After etching, the

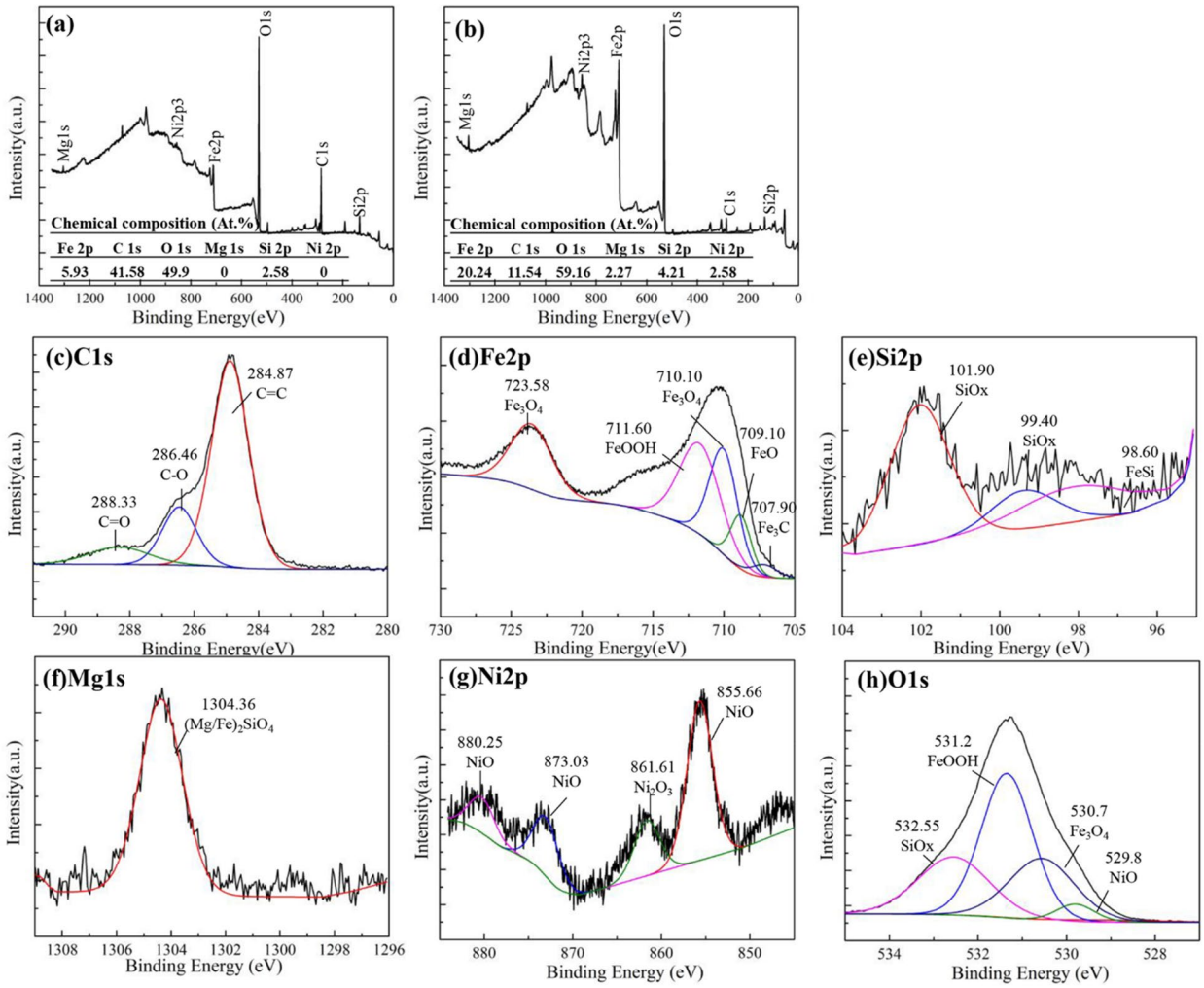

Fig. 5 XPS spectra of the elements on the rubbing surface of disk before etching **a** the full spectra, **c** C 1s and after etching: **b** the full spectra, **d** Fe 2p, **e** Si 2p, **f** Mg 1s, **g** Ni 2p, and **h** O 1s

atomic content of the C 1s spectra dropped from 42.58 to 11.54%, and Mg and Ni appeared, indicating that the carbon layer on the surface was slightly thicker than 20 nm.

In Fig. 5d, the subpeak at a higher binding energy (Fe2p 1/2) is attributed to Fe_3O_4, while the lower subpeak (Fe2p 3/2) is contributed by Fe_3C, FeO, Fe_3O_4, and FeOOH. The Si2p spectrum reveals that Si exists as SiO_x and FeSi in the tribofilm. The O 1s spectrum after etching is fitted into four subpeaks at binding energy of 529.8 eV (NiO), 530.7 eV (Fe_3O_4), 531.2 eV (FeOOH), and 532.55 eV (SiO_x). It is worth noting that the Mg 1s peak at 1304.36 eV corresponds to $(Mg/Fe)_2SiO_4$, which suggests that the MSH in the composite powder undergoes a chemical reaction with the iron-based surface. The formation mechanism of the MSH tribofilm is closely related to the frictional thermodynamics and its layered structure. When the friction progresses, the layered structure of MSH is destroyed under pressure, releasing a large number of active oxygen atoms and free bonds (Si–O/OH, Mg–O/OH) [9, 20]. These released substances undergo a tribochemical reaction with the metal matrix to form iron oxide, silicon oxide, and magnesium iron compounds to form a self-repairing layer. In contrast, Fig. 5g shows that Ni only exists as NiO and Ni_2O_3, indicating that there is no chemical reaction between Ni and the matrix. The reason why the tribofilm contains Ni is that the plastic flow of the friction surface causes nano-Ni to enter the matrix, which is a physical process. This result is consistent with the EDS results of disk and ball surfaces lubricated with Ni. The hardness of the ball (62–64 HRC) restricts plastic flow, and the hardness of the disk (32–35 HRC) easily produces plastic flow, so a large amount of Ni can only be detected on the surface of the disk. Combining the spectrum and elemental content after etching, the tribofilm formed by the MSH/Ni composite powder as an additive on the rubbing surface is

observed to be mainly composed of Fe_3O_4, FeOOH, SiO_x, and NiO.

3.4 Synergistic Effect

These results suggest that the friction performance of the composite powder is better than that of the single powder, and this is attributed to the synergistic effect of MSH and Ni. The MSH and Ni in the composite powders can form a tribofilm on the surface in different ways. To further analyze the synergistic mechanism, friction tests under different loads (60 N, 140 N, and 180 N) were carried out for 2 h. The rotation speed and additive content are the same as the previous tests. As shown in Fig. 6a, when the load is 60 N and 140 N, the composite powder has the best anti-friction performance, and the average friction coefficient with Ni is lower than that with MSH. When the load is 180 N, the anti-friction performance has the following order: MSH < MSH/Ni < Ni. The friction coefficient of MSH is always the highest. This is because MSH mainly forms a tribofilm to improve the anti-wear performance of the mechanical parts, while Ni converts sliding friction to rolling friction to reduce friction. The order of the average WSA in Fig. 6b at 60 N and 140 N is MSH/Ni > MSH > Ni, and the average WSA of MSH is approximately twice that of MSH/Ni and Ni. When the load is 180 N, MSH/Ni still has the best anti-wear performance, but the WSA of Ni is larger than that of MSH. The optical images of the wear scar lubricated with MSH/Ni under different loads are shown in Fig. 6c–e. When the load is 60 N and 140 N, the shape of the wear scar is elliptical.

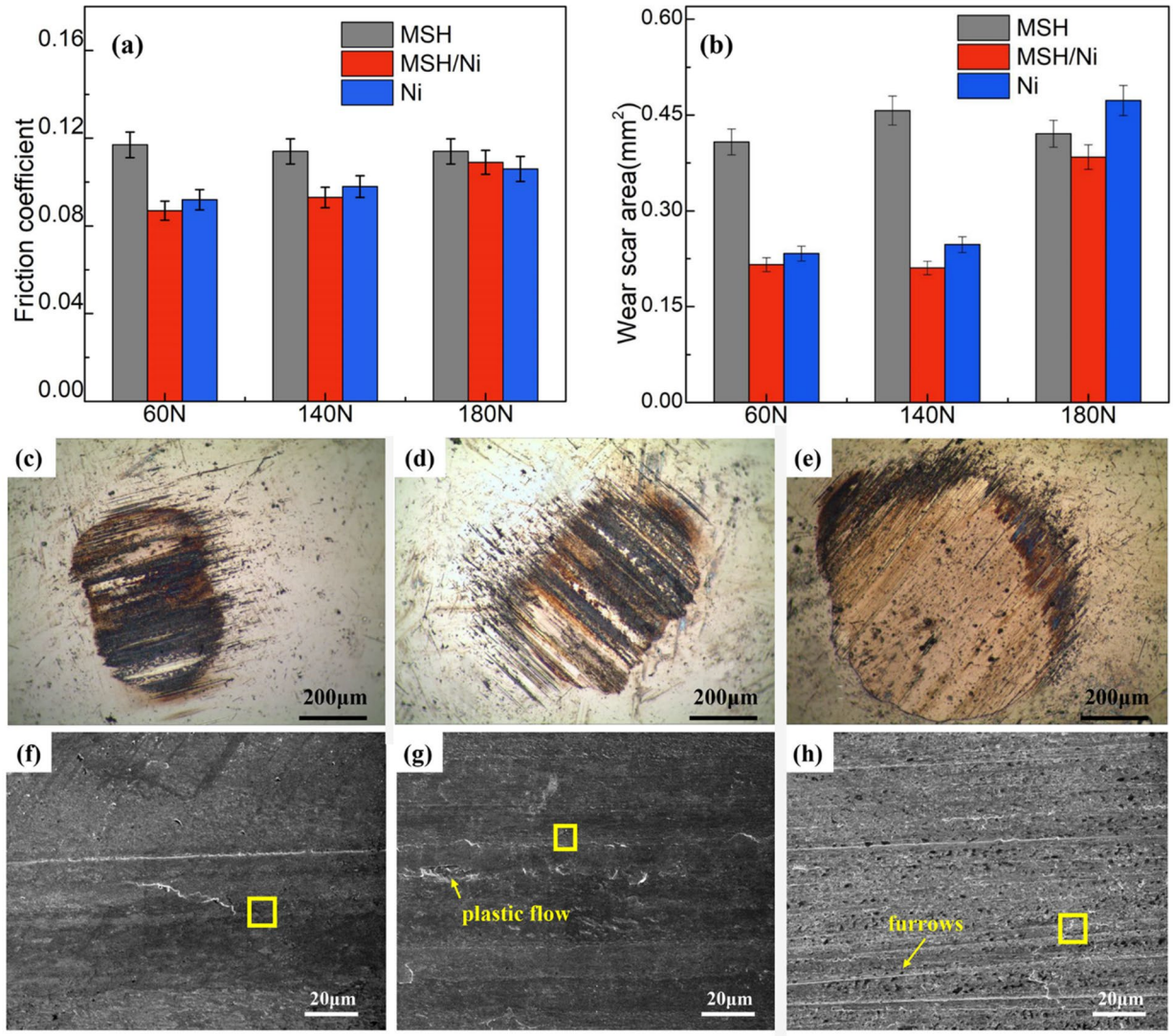

Fig. 6 The average friction coefficient (**a**) and average wear scar area (**b**) of different additives under different loads; Optical and SEM images of the wear scars under different loads: **c**, **f** 60 N, **d**, **g** 140 N, and **e**, **h** 180 N

This phenomenon indicates that the contact area in the sliding direction is smaller than the contact area in the vertical sliding direction, which is due to the wear of the disk in the sliding direction [39] and the lubrication effect of the additive in the sliding direction. When the load is 180 N, the area of wear scar increases obviously, and the shape is close to a circle, which means that high load causes lubrication failure.

As shown in Fig. 6f–h, the MSH/Ni surface is very smooth at 40 N, and obvious plastic flow marks appear on the surface at 140 N. There are many furrows at 180 N, and the surface morphology is completely different from that under low load. The EDS results in Table 2 show that the worn surface contains elemental Mg, Si, and Ni when the load is 180 N, but does not contain Mg when the load is 140 N. When the load is 60 N, there is only elemental Fe, O, and Ni on the worn surface, and the Ni content is lower than that at 140 N. These results indicate that the synergistic mechanism of MSH/Ni composite powder is affected by the load. Combined with the EDS and XPS results in the 100-N long-term test, the synergistic mechanism is summarized in Fig. 7.

When the load is low (60–140 N), the spherical micro-Ni in the composite powder mainly acts as microbearings, converting the sliding friction between the friction pairs into rolling friction, thereby reducing wear. Additionally, the tribofilm containing Ni is formed under the action of surface plastic flow, and the Ni content is positively correlated with load. Destroying the layered MSH structure is a necessary condition for the formation of a tribofilm [40]. However, under low load, micro-Ni disperses the pressure between the friction pairs, which makes it difficult for small-sized MSH to decompose to form a magnesium-containing tribofilm during the initial stage of wear. As the friction and wear progress, micro-Ni will still exert pressure on MSH to destroy its structure, allowing MSH to release free bonds (Si–O/OH, Mg–O/OH) and chemically react with the substrate to form a tribofilm. When the load is too large (180 N) and exceeds the carrying capacity of the Ni particles, the spherical Ni loses its function as microbearings and spreads on the friction surface instead. At the same time, MSH breaks and releases free bonds (Si–O/OH, Mg–O/OH) under pressure, forming a tribofilm containing FeOOH, Fe_3O_4, and SiO_x. In short, the MSH/Ni composite powder makes full use of the different anti-wear mechanisms of MSH and Ni so that it has better friction properties.

Table 2 Elemental composition of the worn surfaces under different loads

Load	Content (at%)				
	Fe	O	Mg	Ni	Si
60 N	65.90	33.39	0	0.71	0
140 N	66.02	31.33	0	2.19	0.46
180 N	68.03	27.19	1.18	1.94	0.76

To further evaluate the tribological performance of MSH/Ni composite powder, the commercial zinc dialkyl dithiophosphate (ZDDP) and molybdenum dithiocarbamate (MoDTC) lubricant additives were used to contrast with composite powder. Figure 8a shows that MSH/Ni composite powder has the best anti-wear performance. The average WSA of ZDDP is 0.659, which is 57.28% larger than that of MSH/Ni, while the average WSA of MoDTC is only 1.91% larger than the composite powder. However, ZDDP has the best anti-friction performance, and the friction coefficient vs. time curve is shown in Fig. 8b. There are many fluctuation peaks in the FC curve of ZDDP, and the overall trend of the friction coefficient is going upward, which indicates that the lubrication effect of ZDDP often fails at 180 N, and the wear is aggravated. The friction coefficients of MSH/Ni and MoDTC have the same changing trend. First, the friction curve jumps during the running-in period. As the running-in period ends, the friction coefficient decreases, and then the additive begins to form a tribofilm, which causes the friction

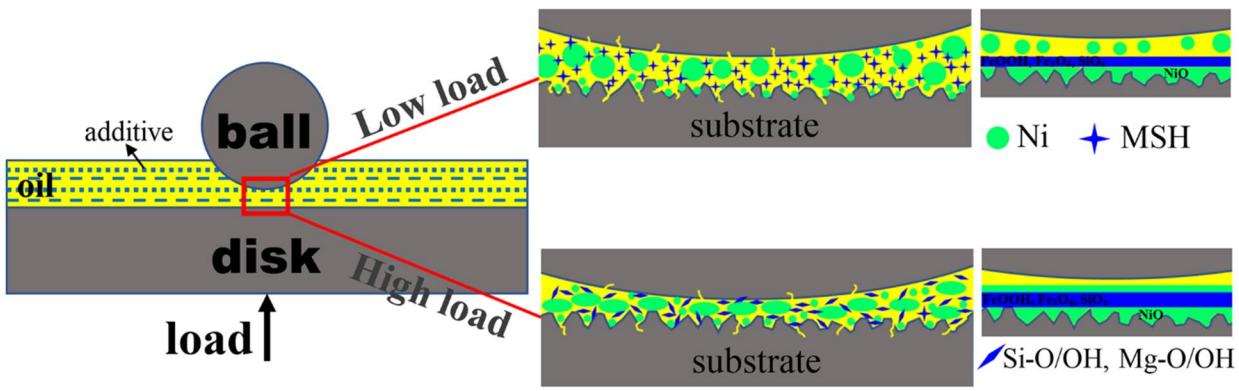

Fig. 7 Formation mechanism of the tribofilm generated by the MSH/Ni composite under different loads

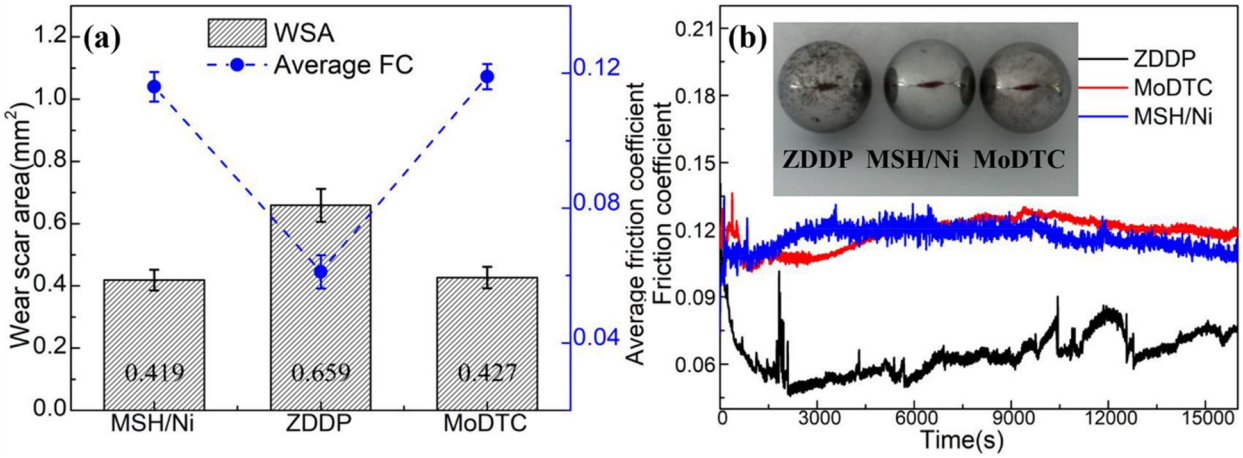

Fig. 8 **a** Average FC and WSA with different oil samples; **b** Friction coefficient curves and optical image of the balls

coefficient to increase and finally gradually decreases with the formation of the tribofilm. Although commercial lubricant additives also have good tribological properties, they contain elements, such as S and P, which not only pollute the environment but also corrode metals. Figure 8b shows the optical images of the balls with different additives stored for one week after the wear test. Obviously, the corrosion degree of the steel balls is ZDDP > MoDTC > MSH/Ni. Therefore, MSH/Ni composite powder is a green lubricating additive with excellent anti-wear properties.

4 Conclusion

In this study, MSH/Ni composite was prepared by mechanical ball milling, and its tribological properties as an oil-based additive in steel–steel contact were investigated. The MSH/Ni composite as a lubricant additive exhibits friction reduction (15.1%) and superior anti-wear (78.13%) performance compared to the MSH and Ni alone. During the friction process, MSH releases free bonds to generate a tribochemical reaction with the matrix to form a tribofilm, while Ni forms a tribofilm through surface plastic flow. Under the synergistic effect of the MSH and Ni, the MSH/Ni composite powder can form a smoother tribofilm mainly containing Fe_3O_4, FeOOH, SiO_x, and NiO on the surface. Furthermore, the excellent friction performance of the MSH/Ni composite powder is mainly attributed to the microbearing effect of Ni. Furthermore, under heavy load (180 N), the excellent friction performance is due to the self-repairing effect of MSH. Compared with ZDDP and MoDTC, MSH/Ni composite powder exhibits better anti-wear performance and is more friendly to the environment and to metal parts. The findings in this paper provide a novel insight for the synergistic effects of compound additions, and these results can be used as a reference when designing composite materials.

Acknowledgements We would like to the National Natural Science Foundation of China (No. 51675357) for their support in this work.

References

1. Dassenoy, F.: Nanoparticles as additives for the development of high performance and environmentally friendly engine lubricants. Tribol. Online **14**(5), 237–253 (2019). https://doi.org/10.2474/trol.14.237
2. Dai, W., Kheireddin, B., Gao, H., Liang, H.: Roles of nanoparticles in oil lubrication. Tribol. Int. **102**, 88–98 (2016). https://doi.org/10.1016/j.triboint.2016.05.020
3. Dixena, R.K., Sayanna, E., Badoni, R.P.: A study on tribological behaviours of ZDDP in polymer thickened lubricating greases. Lubr. Sci. **28**(3), 177–186 (2016). https://doi.org/10.1002/ls.1324
4. Mamedova, A.K., Farzaliev, V.M., Kyazim-zade, A.K.: New sulfur-, nitrogen-, and boron-containing multifunctional alkylphenolate additives for motor oils. Petrol. Chem. **57**(8), 718–721 (2017). https://doi.org/10.1134/s0965544117080072
5. Wang, B., Zhong, Z., Qiu, H., Chen, D., Li, W., Li, S., Tu, X.: Nano serpentine powders as lubricant additive: tribological behaviors and self-repairing performance on worn surface. Nanomaterials-Basel (2020). https://doi.org/10.3390/nano10050922
6. Yu, H.L., Xu, Y., Shi, P.J., Wang, H.M., Wei, M., Zhao, K.K., Xu, B.S.: Microstructure, mechanical properties and tribological behavior of tribofilm generated from natural serpentine mineral powders as lubricant additive. Wear **297**(1–2), 802–810 (2013). https://doi.org/10.1016/j.wear.2012.10.013
7. Zhang, B., Xu, Y., Gao, F., Shi, P., Xu, B., Wu, Y.: Sliding friction and wear behaviors of surface-coated natural serpentine mineral powders as lubricant additive. Appl. Surf. Sci. **257**(7), 2540–2549 (2011)
8. Zhang, Y.W., Li, Z.P., Yan, J.C., Ren, T.H., Zhao, Y.D.: Tribological behaviours of surface-modified serpentine powder as lubricant additive. Ind. Lubr. Tribol. **68**(1), 1–8 (2016). https://doi.org/10.1108/Ilt-01-2013-0005
9. Zhang, B.S., Xu, B.S., Xu, Y., Ba, Z.X., Wang, Z.Z.: An amorphous Si-O film tribo-induced by natural hydrosilicate powders

on ferrous surface. Appl. Surf. Sci. **285P**, 759–765 (2013). https://doi.org/10.1016/j.apsusc.2013.08.123
10. Wu, J.W., Wang, X., Zhou, L.H., Wei, X.C., Wang, W.R.: Formation factors of the surface layer generated from serpentine as lubricant additive and composite reinforcement. Tribol. Lett. **65**(3), 93 (2017). https://doi.org/10.1007/s11249-017-0873-1
11. Du Breuil, C., César-Pasquier, L., Dipple, G., Blais, J.F., Iliuta, M.C., Mercier, G.: Mineralogical transformations of heated serpentine and their impact on dissolution during aqueous-phase mineral carbonation reaction in flue gas conditions. Minerals (2019). https://doi.org/10.3390/min9110680
12. Gualtieri, A.F., Lusvardi, G., Pedone, A., Di Giuseppe, D., Zoboli, A., Mucci, A., Zambon, A., Filaferro, M., Vitale, G., Benassi, M., Avallone, R., Pasquali, L., Lassinantti Gualtieri, M.: Structure model and toxicity of the product of biodissolution of chrysotile asbestos in the lungs. Chem. Res. Toxicol. **32**(10), 2063–2077 (2019). https://doi.org/10.1021/acs.chemrestox.9b00220
13. Boyles, M.S.P., Poland, C.A., Raftis, J., Duffin, R.: Assessment of the physicochemical properties of chrysotile-containing brake debris pertaining to toxicity. Inhal. Toxicol. **31**(8), 325–342 (2019). https://doi.org/10.1080/08958378.2019.1683103
14. Skuland, T., Maslennikova, T., Lag, M., Gatina, E.M., Serebryakova, M.K., Trulioff, A.S., Kudryavtsev, I.V., Klebnikova, N., Kruchinina, I., Schwarze, P.E., Refsnes, M.: Synthetic hydrosilicate nanotubes induce low pro-inflammatory and cytotoxic responses compared to natural chrysotile in lung cell cultures. Basic Clin. Pharmacol. Toxicol. **126**(4), 374–388 (2020). https://doi.org/10.1111/bcpt.13341
15. Gazzano, E., Foresti, E., Lesci, I.G., Tomatis, M., Riganti, C., Fubini, B., Roveri, N., Ghigo, D.: Different cellular responses evoked by natural and stoichiometric synthetic chrysotile asbestos. Toxicol. Appl. Pharmacol. **206**(3), 356–364 (2005). https://doi.org/10.1016/j.taap.2004.11.021
16. Gazzano, E., Turci, F., Foresti, E., Putzu, M.G., Aldieri, E., Silvagno, F., Lesci, I.G., Tomatis, M., Riganti, C., Romano, C., Fubini, B., Roveri, N., Ghigo, D.: Iron-loaded synthetic chrysotile: a new model solid for studying the role of iron in asbestos toxicity. Chem. Res. Toxicol. **20**(3), 380–387 (2007). https://doi.org/10.1021/tx600354f
17. Yu, R., Liu, F., Ren, H., Wu, J., Zhang, X.: Formation of magnesium hydrosilicate nanomaterials and its applications for phosphate/ammonium removal. Environ. Technol. **39**(17), 2162–2167 (2018). https://doi.org/10.1080/09593330.2017.1351495
18. Gao, K., Chang, Q., Wang, B., Zhou, N., Qing, T.: The tribological performances of modified magnesium silicate hydroxide as lubricant additive. Tribol. Int. **121**, 64–70 (2018). https://doi.org/10.1016/j.triboint.2018.01.022
19. Wang, B., Chang, Q.Y., Gao, K., Fang, H.R., Zhou, N.N.: The synthesis of magnesium silicate hydroxide with different morphologies and the comparison of their tribological properties. Tribol. Int. **119**, 672–679 (2017). https://doi.org/10.1016/j.triboint.2017.11.020
20. Gao, K., Chang, Q.Y., Wang, B., Zhou, N.N., Qing, T.: The purification and tribological property of the synthetic magnesium silicate hydroxide modified by oleic acid. Lubr. Sci. **30**(7), 377–385 (2018). https://doi.org/10.1002/ls.1428
21. Zhang, Q., Wu, B., Song, R., Song, H., Zhang, J., Hu, X.: Preparation, characterization and tribological properties of polyalphaolefin with magnetic reduced graphene oxide/Fe_3O_4. Tribol. Int. (2020). https://doi.org/10.1016/j.triboint.2019.105952
22. Deshpande, P., Dassenoy, F., Minfray, C., Jenei, I.Z., Le Mogne, T., Thiebaut, B.: Effect of adding TiO_2 nanoparticles to a lubricant containing MoDTC on the tribological behavior of steel/steel contacts under boundary lubrication conditions. Tribol. Lett. (2020). https://doi.org/10.1007/s11249-020-1278-0
23. Meng, Y., Su, F.H., Chen, Y.Z.: Nickel/multi-walled carbon nanotube nanocomposite synthesized in supercritical fluid as efficient lubricant additive for mineral oil. Tribol. Lett. (2018). https://doi.org/10.1007/s11249-018-1088-9
24. Du, P., Chen, G., Song, S., Chen, H., Li, J., Shao, Y.: Tribological properties of muscovite, CeO_2 and their composite particles as lubricant additives. Tribol. Lett. (2016). https://doi.org/10.1007/s11249-016-0676-9
25. Daji, W., Dachuan, Z., Huafeng, L., Guoxu, C.: Tribological properties of muscovite/La_2O_3 composite powders as lubricant additives. Tribol. Trans. **58**(4), 577–583 (2015). https://doi.org/10.1080/10402004.2014.996309
26. Du, P., Chen, G., Song, S., Zhu, D., Wu, J., Chen, P., Chen, H.: Preparation and tribological properties of Cu-doped muscovite composite particles as lubricant additive. Chem. Res. Chin. Univ. **33**(3), 430–435 (2017). https://doi.org/10.1007/s40242-017-6418-1
27. Zhao, F., Bai, Z., Fu, Y., Zhao, D., Yan, C.: Tribological properties of serpentine, La(OH)3 and their composite particles as lubricant additives. Wear **288**, 72–77 (2012). https://doi.org/10.1016/j.wear.2012.02.009
28. Zhang, B.S., Xu, B.S., Xu, Y., Ba, Z.X., Wang, Z.Z.: Lanthanum effect on the tribological behaviors of natural serpentine as lubricant additive. Tribol. Trans. **56**(3), 417–427 (2013). https://doi.org/10.1080/10402004.2012.758332
29. Zhang, B.-S., Xu, B.-S., Xu, Y., Gao, F., Shi, P.-J., Wu, Y.-X.: CU nanoparticles effect on the tribological properties of hydrosilicate powders as lubricant additive for steel–steel contacts. Tribol. Int. **44**(7–8), 878–886 (2011). https://doi.org/10.1016/j.triboint.2011.03.002
30. Cheng, L., Hu, E., Chao, X., Zhu, R., Hu, K., Hu, X.: MoS2/montmorillonite nanocomposite: preparation, tribological properties, and inner synergistic lubrication. Nano Brief Rep. Rev. (2019). https://doi.org/10.1142/s1793292018501448
31. Nan, F., Zhou, K.H., Liu, S., Pu, J.B., Fang, Y.H., Ding, W.X.: Tribological properties of attapulgite/La_2O_3 nanocomposite as lubricant additive for a steel/steel contact. Rsc Adv. **8**(30), 16947–16956 (2018). https://doi.org/10.1039/c8ra02835d
32. Nan, F., Xu, Y., Xu, B.S., Gao, F., Wu, Y.X., Li, Z.G.: Tribological performance of attapulgite nano-fiber/spherical nano-Ni as lubricant additive. Tribol. Lett. **56**(3), 531–541 (2014). https://doi.org/10.1007/s11249-014-0430-0
33. Wu, X., Yang, L., Zhou, Y., Cao, Y.: Tribological properties of ultrafine-palygorskite/copper composite powder as lubricant additive. CAILIAO GONGCHENG J. Mater. Eng. **46**(9), 88–94 (2018). https://doi.org/10.11868/j.issn.1001-4381.2016.001507
34. Mobasher, A., Khalil, A., Khashaba, M., Osman, T.: Effect of MWCNTs/Talc powder nanoparticles on the tribological and thermal conductivity performance of calcium grease. Ind. Lubr. Tribol. **72**(1), 9–14 (2020). https://doi.org/10.1108/ILT-03-2019-0102
35. Liu, Y., Xin, L., Zhang, Y., Chen, Y., Zhang, S., Zhang, P.: The effect of Ni nanoparticles on the lubrication of a DLC-based solid-liquid synergetic system in all lubrication regimes. Tribol. Lett. (2017). https://doi.org/10.1007/s11249-017-0814-z
36. Chen, Y., Zhang, Y., Zhang, S., Yu, L., Zhang, P., Zhang, Z.: Preparation of nickel-based nanolubricants via a facile in situ one-step route and investigation of their tribological properties. Tribol. Lett. **51**(1), 73–83 (2013). https://doi.org/10.1007/s11249-013-0148-4
37. Rajendhran, N., Palanisamy, S., Shyma, A.P., Venkatachalam, R.: Enhancing the thermophysical and tribological performance of gear oil using Ni-promoted ultrathin MoS_2 nanocomposites. Tribol. Int. **124**, 156–168 (2018). https://doi.org/10.1016/j.triboint.2018.03.030

38. Erdemir, A., Ramirez, G., Eryilmaz, O.L., Narayanan, B., Liao, Y., Kamath, G., Sankaranarayanan, S.K.: Carbon-based tribofilms from lubricating oils. Nature **536**(7614), 67–71 (2016). https://doi.org/10.1038/nature18948
39. Wang, W., Zhang, G.L., Xie, G.X.: Ultralow concentration of graphene oxide nanosheets as oil-based lubricant additives. Appl. Surf. Sci. **498**, 146683 (2019). https://doi.org/10.1016/j.apsusc.2019.143683
40. Chang, Q.Y., Wang, B., Gao, K.: Pressure-dependent antiwear mechanisms of synthetic magnesium silicate hydroxide nanoparticles. Tribol. Int. **135**, 230–236 (2019). https://doi.org/10.1016/j.triboint.2019.03.016